6th International Conference on Advances in Experimental Structural Engineering
11th International Workshop on Advanced Smart Materials and Smart Structures Technology
August 1-2, 2015, University of Illinois, Urbana-Champaign, United States

On the study of the in-situ thermal stress measurement using a Hole-Drilling method

Xuan Zhu[1], Francesco Lanza di Scalea[2], Mahmood Fateh[3]

1 *Graduate student researcher, Dept Structural Engineering, University of California, San Diego, USA. E-mail: xuz009@ucsd.edu*
2 *Professor, Dept Structural Engineering, University of California, San Diego, USA. E-mail: flanza@ucsd.edu*
3 *Office of Research and Development, Federal Railroad Administration, Washington, DC, USA E-mail: mahmood.fateh@dot.gov*

ABSTRACT
Stress relaxation tests have been widely used for residual stress determination. Especially, the hole drilling test procedure, as a semi destructive test procedure, is capable to measure the residual stresses close to the specimen surfaces, along the in plane directions. The residual stresses are typically computed based on the relieved strains with the calibration coefficients. Inspired by the stress relaxation philosophy, an investigation on thermal stress measurement, in particular for the Continuous Welded Rail (CWR), by using the hole drilling test procedure is conducted in this paper. First, a 3-D finite element model is established to verify the feasibility of using the standardized test to measure the thermal stress, by comparing the computed stress relaxation based on the hole-drilling test with the applied uniaxial thermal stress. To improve the computation accuracy, a novel differential analysis framework is proposed to update the calibration coefficients by more realistic simulations. Two sets of experiments have been carried out on the free-to-expand rail tracks and the ones under thermal load. The relieved stresses are computed with the updated calibration coefficients. The final results illustrate that the proposed models would be promising to characterize in-situ thermal stress with appropriate residual stress compensation.

KEYWORDS: *Hole drilling method, finite element analysis, thermal stress, residual stress*

1. INTRODUCTION

The hole-drilling method, as a semi destructive test procedure first introduced by Mathar in 1930s [1], is the most widely used method to determine the near-surface residual stresses in industry. It features with good accuracy and reliability [2], ASTM standardized test procedures [3], and convenient practical implementation [4]. The small drilled holes from the drilling process are often tolerable or repairable [5]. The general procedure for hole-drilling method includes three steps: 1 drill a small hole at the surface of the specimen to relieve the existing stress within localized region; 2 measure the deformation caused by the stress relaxation with the pre-installed strain gage rosette or optical measurement system; 3 compute the residual stress using the deformation field with the calibration coefficients.

Early works in 1960s and 1970s on the hole-drilling strain-gage method demonstrated its effectiveness and accuracy (better than $\pm 8\%$ in accuracy for steel) on the measurement of the magnitudes and principal direction of residual stresses in elastic materials [2,6]. By then, the calibration coefficients were computed based on experimental results and empirical relationship between the constants and the hole diameter. In 1980s, Schajer [7, 8] proposed a systematic framework to compute the calibration coefficients for the cases with uniformly and non-uniformly distributed residual stress along the hole depths, based on the principle of superposition and axisymmetric finite element models. Aoh and Wei extended the framework by using a 3-D finite element model for integral method and verified the coefficients with the experimental results [9,10]. On the other hand, several optical techniques, such as Moire interferometry [11,12], electronic speckle pattern interferometry (ESPI) [13,14] and digital imaging correlation [15], were introduced to evaluate the full deformation field with the hole-drilling method, in alternation of strain gage rosette.

Through these studies, the hole-drilling method is a well-established standardized test procedure with satisfactory accuracy to measure the residual stress close to the surface of the specimen. The specific application of interest to the present study is the measurement of thermal loads in Continuous-Welded Rail, which is still an unresolved problem in railroad maintenance today. Thermal stresses develop due to constrained thermal

expansion of the welded track. In particular, tensile stresses develop under cold weather, whereas compressive stresses develop under warm weather. Excessive tensile stresses can develop fractures, and excessive compressive stresses can induce buckling. Both cases are high-priority safety hazards in railroad transportation. Buckling in hot weather (the sunkink) had been responsible for over 57M dollars lost from 2006-2011 and caused 3.4% of derailments and 12.7 cars derailed per derailments from 2000-2010 [16]. The well-known formula that governs the thermal loads in CWR is [17].

$$P=\alpha E A (T-NT) \tag{1.1}$$

, where P is the thermal load, α is the coefficient of thermal expansion of steel, E is the Young's Modulus of steel, A is the rail cross-sectional area, T is the rail temperature, and NT is the so-called 'rail Neutral Temperature'. Knowledge of the rail Neutral Temperature, which corresponds to the rail temperature when the rail has zero thermal stress, is of outmost importance to rail engineers. This paper explores the hole-drilling strain-gage method as a possible solution to measure the in-situ thermal stresses in rails and estimate the rail neutral temperature. As a small hole drilled, the thermal stress and residual stress of the localized region would be relieved simultaneously. In this study, the thermal stresses are computed by subtracting the statistical mean value of the residual stresses from the total stress relaxation.

This article is organized as follows: section 2 reviews the essentials of the hole-drilling strain-gage method; section 3 studies the feasibility of applying the hole-drilling test procedure to the thermal load measurement and computes the updated sets of calibration coefficients; the experimental setups and results are discussed in section 4 and the paper concludes in section 5.

2. REVIEW OF THE HOLE-DRILLING STRAIN-GAGE METHOD

In a typical hole-drilling strain-gage test procedure, a series of gentle mechanical and chemical treatments would first be applied on the specimen surface to ensure the effective load transfer and a clean environment for adhesive curing [4]. Locations close to the edges or structural irregularities should be avoided in order to eliminate the boundary effects on the stress relaxation. Special standardized strain gage rosettes with gage circle surrounded by 3 single or pairs of gage elements, as shown in Fig. 2.1, would be bonded to the prepared surface. Depending on the locations and applications with requirements on strain sensitivity and thermal stability, the choices of the gage patterns and sizes can be made. During the drilling procedure, the strain readings would be recorded at each incremental depth, which is determined from the gage size and the assumption of a uniform or non-uniform stress distribution along the drilling depth. To compute the residual stress along the hole depth, the relieved strains would be converted to the stress relaxation with the calibration coefficients provided in the ASTM standard [3].

To compute the in-plane residual stresses from the relieved strains, a critical assumption is made such that the stress and strain distributions around the blind-hole are similar to the ones around a through-hole in an infinite plate [4,7]. Considering the case of a through-hole within a thin infinite linear elastic plate subjected to a uniform uniaxial residual stress σ_x, the stress distribution around a circular hole was solved by Kirsch in 1890s [18]. By subjecting the stress state before drilling from the stress state after drilling, it yields the stress relaxation caused by hole-drilling process. The relieved radial strains at point $P(R,\alpha)$, where R stands for the radius and α represents the angle in cylindrical coordinate representation, can be computed based on linear elasticity as:

$$\varepsilon_{rr} = \sigma_x(A + B\cos 2\alpha) \tag{2.1}$$

, where σ_x is the uniaxial residual stress, $A = -\frac{(1+\nu)}{2E}\left(\frac{1}{r^2}\right)$, $B = -\frac{(1+\nu)}{2E}\left[-\frac{3}{r^4} + \frac{4}{r^2(1+\nu)}\right]$, $r = \frac{R}{R_0}$, R_0 is hole radius, R is arbitrary radius from hole center, α is the angle regards to x axis, E and ν is the Young's modulus and Possion's ratio of the specimen. Only the radial term is considered since the strain gage rosettes are designed with radially oriented grids to measure the relieved radial strain. For a biaxial residual stress state case, the relieved radial strain can be computed as:

$$\varepsilon_r = A(\sigma_x + \sigma_y) + B(\sigma_x - \sigma_y)\cos 2\alpha \tag{2.2}$$

, where σ_x and σ_y are the residual stresses along x and y direction. Equation (2.2) highlights the relationship between the biaxial residual stress state and the relieved radial strain for a through-hole case. With a theoretical approximation, researchers demonstrated that the relationship between the relieved stresses and strains for the

blind-hole case follows the same format as Eq. (2.2). With no close form analytical formulations, the constants A and B for the blind-hole case can be calibrated with experiments [6] and finite element models [7-10]. In most of the finite element approaches, a structure under hydrostatic ($\sigma_x = \sigma_y$) and deviatoric ($\sigma_x = -\sigma_y$) stress state would be simulated to compute A (or a) and B (or b) respectively, where a and b are derived from A and B with less material dependence. The superposition principle to find the relieved strains due to stress redistribution for a uniformly distributed stress case is shown in Fig. 2.2 [7]: the load case (a) represents the state before drilling, and the load at the virtual hole boundary exists for self-equilibrium; the load case (c) shows the stress state after drilling, in which the normal and shear stresses along the hole boundary vanish to be traction free; the load case (b) corresponds to the stress redistribution due to drilling and the deformation field is captured by the rosette. By modeling the load case (b), the deformation led by stress redistribution of hole-drilling procedure can be computed.

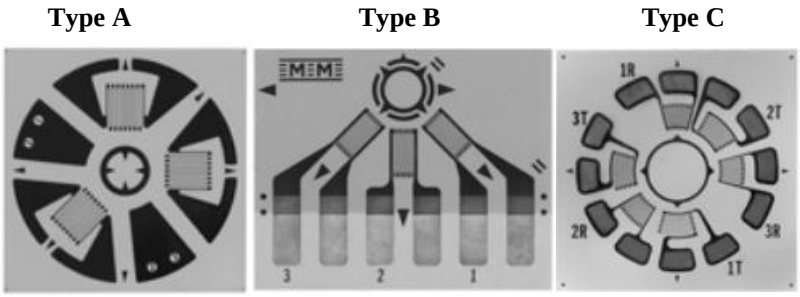

Figure 2.1 Type A, B and C Hole-Drilling Rosettes (resource from Micro-Measurements)

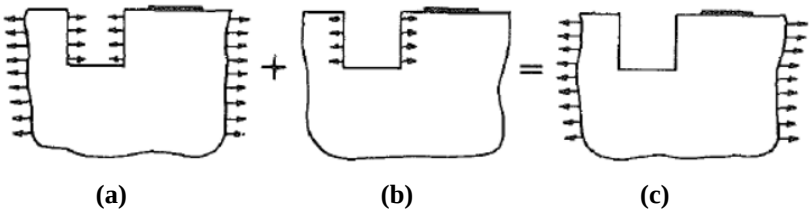

Figure 2.2 Superposition of loadings to find the strain relaxation due to hole drilling:
(a) original state; (b) Stress change due to drilling; (c) final state

3. FINITE ELEMENT ANALYSIS TO DETERMINE THE CALIBRATION COEFFICIENT

A convergence study for the purpose of mesh refinement is conducted on a 2-D through-hole plate subjected to a uniform uniaxial load. The theoretical results for the stress distribution around the hole can be computed by using the Kirsch solution as shown in Fig. 3.1 (a) and (c). This analysis covers the range of radius from the hole radius to the boundary of the strain gage area, and the angle ranged from 0 to 90 degrees by taking advantage of the structural symmetry. On the other hand, the stress distributions of σ_{xx} and σ_{yy} from the 2-D finite element model are shown in Fig. 3.1 (b) and (d). The finite element model is setup as a quarter of a plate with a hole in the center under uniform uniaxial load using the plane stress approximation. Both the analytical and numerical results on the stress distribution agree very well. Furthermore, a parametric study on the mesh refinement is executed on the finite element models from Mesh 1 to Mesh 4 with the mesh size in ascending order. The results of the analytical model and the mesh refinements along the x axis and y axis of the plate are shown in Fig. 3.2. The results from Mesh 1 and Mesh 2 are well aligned with the theoretical result, while large discrepancies are observed in the coarser meshes of Mesh 3 and Mesh 4. In general, the larger the mesh size is, the more discrepancies would be found. Mesh 1 would be used as a reference for mesh configurations in all the 3-D models.

To the best knowledge of the authors, there is no existing work on the thermal stress measurement using the hole-drilling method. Thus, a study of feasibility on applying the hole-drilling test procedure to characterize the thermal stress is carried out. A two-step analysis based on 3-D finite element models is conducted to simulate the hole-drilling implementation on a thermal stress case (neglecting the residual stress). In the 1st step, a temperature variation is applied to a plate constrained along x axis (u=0 at the boundary) and free to expand along y axis as shown in Fig. 3.3 (a), in which the thermal stress builds up to a compressive stress state (-86.1

MPa). The reference temperature of 40℃ is set as the neutral temperature corresponding to the zero stress state and the target temperature of 75℃ is the upper limit rail temperature in the experiments. In the 2nd step, the stress and strain fields from step 1 are projected into a plate with the same geometry and boundary condition setup but a blind hole with specific depth in the plate centre. To satisfy the traction-free condition along the hole boundary, the stress field redistributes which leads to a final displacement field different from the one of step 1. The deformation field corresponding to the strain gage area of step 2 is extracted and averaged to compute the strain gage readings of this specific hole depth, as shown in Fig. 3.3 (b). This two-step analysis is repeated for 8 incremental hole depths. The stress relaxation computed based on the calibration coefficient from ASTM standard would be compared with the applied thermal stress. The computed relieved stress of σ_x is -86.7 MPa, with a 0.7% error rate compared with the applied thermal stress. The computed relieved stress of σ_y is -1.06 MPa, about 1.2% of the in-situ thermal stress along x axis. The error rates of the stress relaxation on both directions are excellent. Given the in-situ thermal stress and the current rail temperature, the rail neutral temperature can be estimated with a simple calculation based on Eq. (2.1). Through this study, it concludes that the hole-drilling test procedure is capable to measure the thermal stress and the rail neutral temperature, with a prior knowledge of the residual stress.

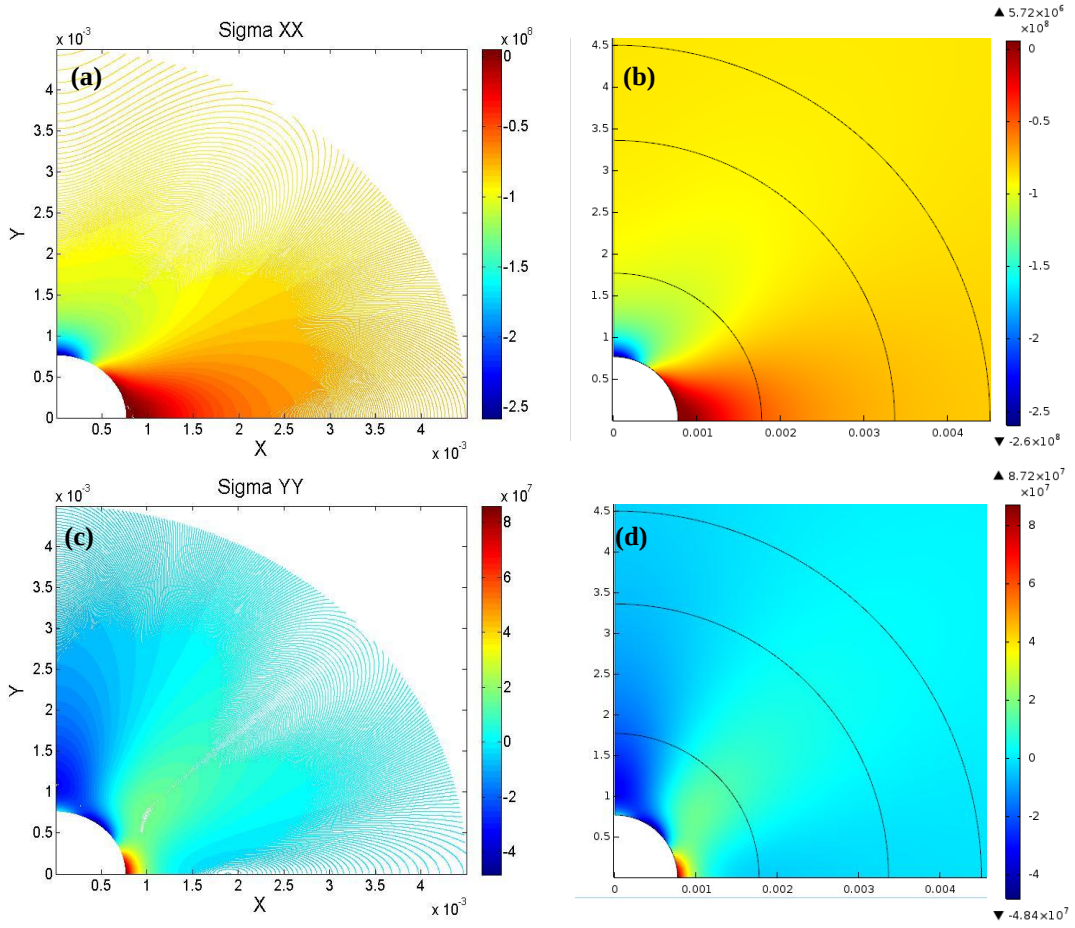

Figure 3.1 Stress distribution around the through hole
(a) analytical σ_{xx}; (b) numerical σ_{xx}; (c) analytical σ_{yy}; (d) numerical σ_{yy}.

To determine the calibration coefficients for the blind-hole uniform stress case, a novel 3-D finite element analysis is conducted based on the mesh configuration optimized in 2-D model. In previous numerical investigation to compute the calibration coefficients for hole-drilling method, the relieved strains were extracted from the model as shown in Fig. 2.2 (b), in which the shear stresses at the hole bottom was not taken into consideration. In the meanwhile, the 2-D axisymmetric model was of a cylindrical geometry and neglected the constrains from the elements on the parallel adjacent planes. In the present study, a differential analysis is proposed to compute the displacement field led by hole-drilling process: a plate with approximately the same thickness as the rail web under hydrostatic/deviatoric stress state is simulated in the 1st step; the plate with a blind hole at specific hole depth under the same load is modeled in the 2nd step. Subtracting the strain gage readings of the 1st step from the ones of the 2nd step would result in the relieved strains due to the stress

relaxation. Knowing the applied stress state, the calibration coefficient of a and b at specific hole depth can be computed. This procedure would be repeated for 8 incremental hole depths and various ratios of hole diameter to gage circle diameter. The resulted calibration coefficients are shown in Table 3.1 and the error rates in percentage as comparison to the ASTM standard are shown in Table 3.2. In general, for a fixed hole diameter to gage circle diameter ratio, the error rates decrease with the incremental hole depths, indicating that there would be less differences between two numerical results for deeper hole depths. This observation is as expected since the deeper the hole depth is, the less effect from the relieved stress on the surface displacement field. The mesh refinement has been conducted and the current mesh size provides a satisfactory accuracy. A further work on comparing the proposed method to compute the calibration coefficients with the other methods is needed. At this stage, the updated calibration coefficients are ready for implementation to compute the stress relaxation from the experiments.

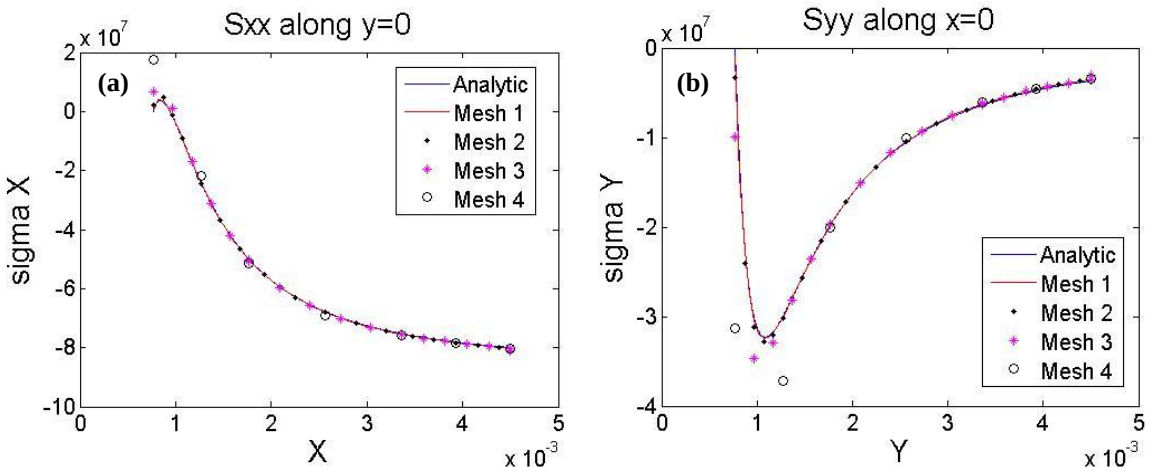

Figure 3.2 Stress distribution around the through hole from analytical and numerical models
(a) σ_{xx} along the x axis; (b) σ_{yy} along the y axis.

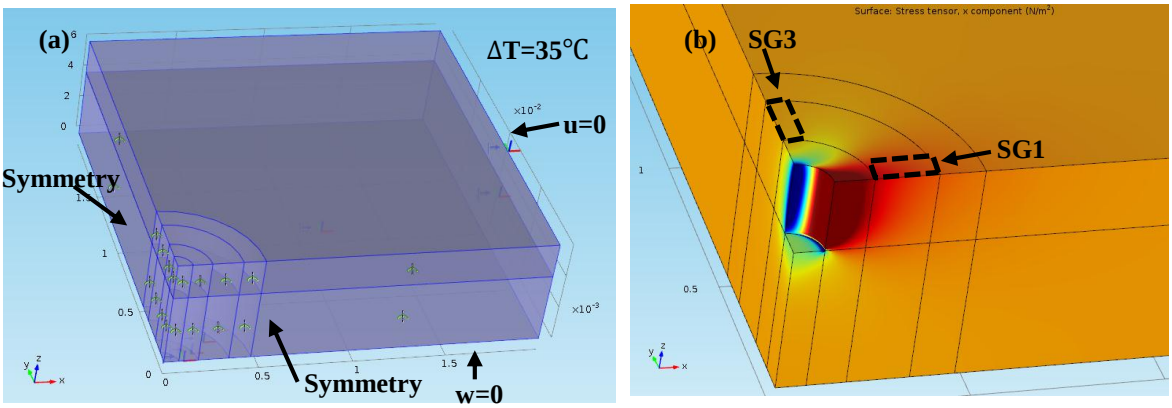

Figure 3.3 (a) the boundary conditions setup in the 1st step
(b) σ_{xx} of the 8th (final) hole depth at the 2nd step and the strain gage locations

4. EXPERIMENTAL SETUP AND RESULTS

The finite element analysis from previous section verifies the feasibility to apply the hole-drilling method on thermal stress measurement, and provides the updated sets of calibration coefficients computed based on more realistic models. To measure the thermal stress in CWRs, the hole-drilling test procedure is proposed as: relieve the residual and thermal stress by drilling a tiny blind hole along the neutral axis on the rail web; record the strain gage readings from the rosette at each hole depth; compute the total stress relaxation and compensate with the residual stress to get the in-situ thermal stress. The residual stress can be estimated from various resources, including the prior measurements and finite element models. The prior measurements can be the residual stress information provided by the manufacturers or determined by the statistics of the residual stress measurements.

In present study, the later method is used as the estimation of the residual stress along the rail neutral axis. In the meanwhile, a uniform residual stress distribution approximation is assumed along the hole depth at the neutral axis, considering the small final depth (2.5 mm for 62UL rosette) and the smooth variation according to historic data [19].

Table 3.1 The calibration coefficients computed from the proposed finite element models

	a					**b**				
	Hole Diameter D0/D					**Hole Diameter D0/D**				
Hole Depth/D	**0.3**	**0.35**	**0.4**	**0.45**	**0.5**	**0.3**	**0.35**	**0.4**	**0.45**	**0.5**
0.05	0.027	0.037	0.050	0.067	0.088	0.053	0.072	0.094	0.121	0.155
0.1	0.060	0.083	0.110	0.143	0.184	0.123	0.164	0.212	0.268	0.332
0.15	0.087	0.118	0.155	0.198	0.247	0.185	0.245	0.313	0.387	0.466
0.2	0.104	0.140	0.182	0.229	0.281	0.231	0.304	0.384	0.468	0.554
0.25	0.113	0.151	0.195	0.244	0.296	0.263	0.344	0.430	0.519	0.607
0.3	0.116	0.156	0.200	0.248	0.301	0.282	0.368	0.458	0.550	0.639
0.35	0.116	0.155	0.200	0.248	0.300	0.293	0.381	0.474	0.567	0.656
0.4	0.114	0.153	0.197	0.244	0.296	0.298	0.388	0.482	0.576	0.664

Table 3.2 The error rate in percentage between the computed calibration coefficients and the ASTM standard

	error rate_a					**error rate_b**				
	Hole Diameter D0/D					**Hole Diameter D0/D**				
Hole Depth/D	**0.3**	**0.35**	**0.4**	**0.45**	**0.5**	**0.3**	**0.35**	**0.4**	**0.45**	**0.5**
0.05	4.11	4.54	6.02	9.30	13.64	8.27	7.83	8.21	10.75	13.81
0.1	5.22	5.02	4.64	6.45	6.70	6.86	6.06	5.85	7.83	7.20
0.15	4.25	4.81	4.64	4.83	5.17	4.93	4.77	4.67	5.19	4.69
0.2	4.05	3.59	4.00	3.70	3.63	3.59	3.48	3.46	3.45	2.86
0.25	3.04	3.63	3.32	2.82	3.10	2.56	2.55	2.34	2.24	1.57
0.3	2.78	3.13	2.59	2.29	2.60	1.81	1.81	1.65	1.35	0.65
0.35	2.42	2.73	2.13	2.19	2.40	0.73	1.10	0.86	0.54	0.15
0.4	2.41	2.34	2.06	1.92	2.05	0.61	0.56	0.21	0.09	-0.39

A typical experiment setup is shown in Fig. 4.1: the hole-drilling assembly sits on a horizontal platform and is fixed by a customized fixture towards the rail web; the journal hole would be first aligned using a microscope to target at the centre of the pre-installed strain gage rosette; a blind hole would then be progressively drilled with the air turbine powered by the compressed air; the strain gage readings at each step are recorded with the strain indicator. Two sets of experiments are conducted on AREAMA 136RE rails. In test 1, the hole-drilling method is applied to determine the residual stresses of 6 locations along the neutral axis on the free-to-expand rail track, as shown in Fig. 4.2(a); the hole-drilling procedure is applied on 4 locations of the 136RE rail track at UCSD/FRA Large-scale rail buckling testbed, where both the residual and thermal stresses would present in test 2, as shown in Fig. 4.2(b). The residual stresses at the neutral axis of 136RE rail tracks are estimated from the results of test 1. In order to measure the thermal stress, the mean value of the residual stresses from test 1 would be applied to compensate the residual stress part of the stress relaxation in test 2. The error rate between the measured and the in-situ thermal stresses would be computed to validate the feasibility of the proposed method on thermal stress characterization.

As shown in Table 4.1, the mean value of the residual stress along x direction (σ_x) at the neutral axis of 136RE rail is -116.3 MPa. From test 2, the measured thermal stresses ($\sigma_{\Delta T\ meas}$) at each tests are computed by subjecting the mean residual stress from test 1 from the total relieved stress, and finally compared with the in-situ thermal stress ($\sigma_{\Delta T\ in-situ}$) provided by the DAQ system of the UCSD/FRA Large-scale rail buckling testbed. From Table 4.2, the errors on thermal stress measurements are ranged from -13 MPa to 3 MPa, corresponding to the errors on neutral temperature estimation ranged from -5.28℃ to 1.22℃. The potential sources caused the errors include: the proposed method ignores the variations of the residual stress from location to location on the neutral axis, which can be fixed by a full investigation involving high statistical population or a potential relationship between σ_x and σ_y; the measurement errors from the experiments might lead to the discrepancies from in-situ thermal stress, such as the rosette misalignment during installation. The strain gage thermal output is another potential problem, even though the gage elements are self-temperature-compensated. The errors of the neutral temperature estimation are generally within ± 5℃ which satisfy the industrial

requirement. Thus, the proposed method has been validated as a potential solution to measure the in-situ thermal stress in CWRs.

During the analysis of two tests, the assumption of uniform stress distribution along the drilling depth is checked for each hole. In most cases, the assumption stands. In the meanwhile, the calculation based on non-uniform stress distribution has been carried out and a smooth linear variation of the residual stress is observed along the hole depth. Further investigation on the uniform and non-uniform stress distribution assumptions is needed.

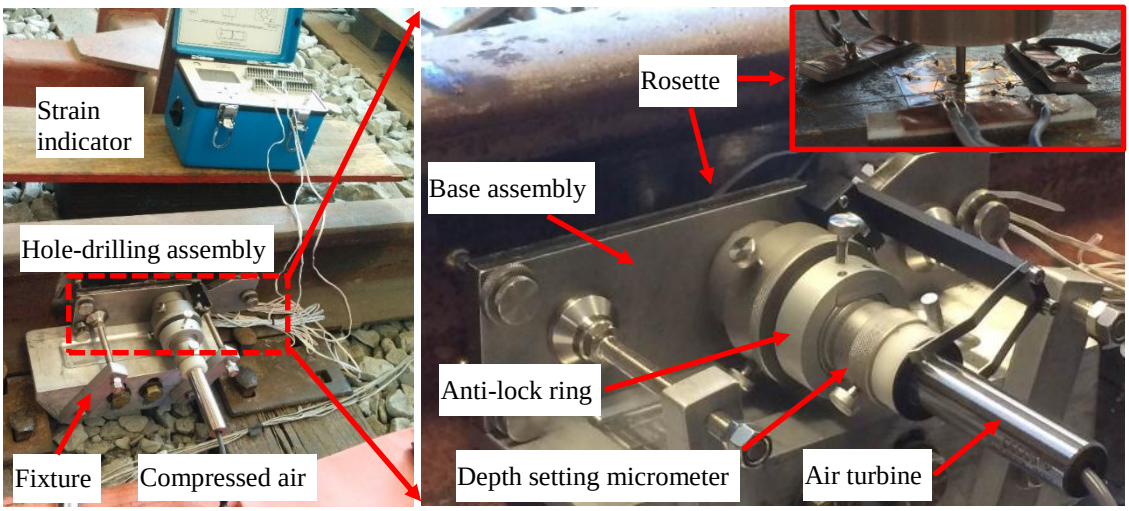

Figure 4.1 The typical experimental setup for the hole-drilling method implementation in CWR

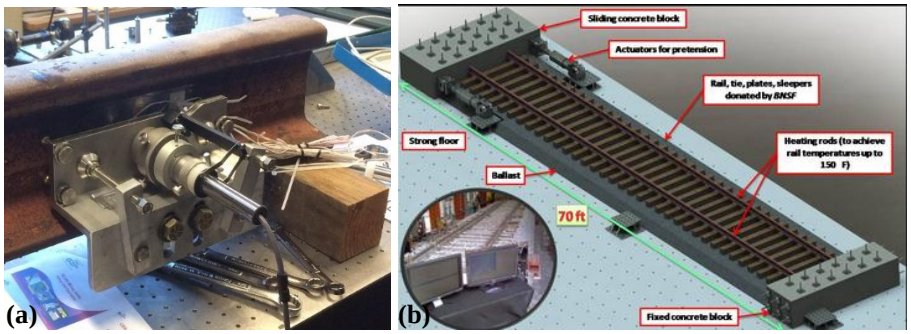

Figure 4.2 The experimental setup for (a) test 1 on the 136RE rail track
(b) test 2 with pre-tensioned rail tracks under the temperature variations

Table 4.1 The residual stresses computed from test 1 based on the updated calibration coefficients

	Test 1					
σ_x (MPa)	-127.864	-123.287	-104.701	-112.792	-119.683	-109.717
σ_y (MPa)	-14.455	-10.548	-25.040	-32.650	-33.375	-41.376

Table 4.2 The residual and thermal stresses computed from test 2 based on the updated calibration coefficients

	Test 2			
σ_x (MPa)	-59.820	-125.069	-86.873	-69.680
σ_y (MPa)	-40.685	-26.234	-25.438	-30.837
$\sigma_{\Delta T\ in-situ}$ (MPa)	69.589	1.972	37.546	43.626
$\sigma_{\Delta T\ meas}$ (MPa)	56.521	-8.728	29.468	46.660
Error (MPa)	-13.068	-10.700	-8.078	3.035

5. CONCLUSION

This paper proposes to implement the hole-drilling method to measure the thermal stress in structural elements, particularly in CWRs. A comparative study is first conducted to check the convergence based on analytical and 2-D finite element models for through-hole cases. Followed by a 2-step finite element analysis, the feasibility of using the standardized test for thermal stress measurement is verified, by comparing the computed stress relaxation based on the hole-drilling test to the applied uniaxial thermal stress. Furthermore, the improved calibration coefficients are updated with differential analysis based on 3-D finite element models which would provide more realistic simulations to the practical applications. The hole-drilling test procedures are done on two sets of experiments to measure the residual stress and determine the thermal stresses, with the updated calibration coefficients. A satisfactory error range of $\pm 5℃$ for the neutral temperature estimation is observed in most cases of test 2, such that the proposed method is validated to measure the in-situ thermal stress in CWRs.

ACKNOWLEDGMENTS

This project is supported by the U.S. Federal Railroad Administration. The Program Manager is Mahmood Fateh from the FRA Office of Research and Development. Special recognition is extended to the Burlington Northern Santa Fe (BNSF) railway for providing in-kind support for the rail tracks and the exchange of technical information.

REFERENCE

1. Mathar, J. (1934). Determination of initial stresses by measuring the deformation around drilled holes. *Trans ASME* **56: 4**, 249–254.
2. Bean, E. M. (1976), Accurate measurement of residual stress in any steel using the centre hole method. *Strain* **12: 3**, 99–106.
3. American Society for Testing and Materials (2008). Determining residual stresses by the hole-drilling strain-gage method. *ASTM Standard test method E837-08*.
4. Vishay Measurements Group, Inc. (1996). Measurement of residual stresses by the hole drilling strain-gage method. *Technical note TN-503-6*.
5. Schajer, G.S. (2010). Hole-Drilling Residual Stress Measurements at 75: Origins, Advances, Opportunities. *Experimental Mechanics*, **50:245**, 253.
6. Rendler, N. J., Vigness, I. (1966). Hole-drilling strain-gage method of measuring residual stresses. *Experimental Mechanics*, **6:12**, 577-586.
7. Schajer, G.S. (1981). Application of finite element calculations to residual stress measurements. *J Eng Mater Technol*, **103: 2**, 157–163.
8. Schajer, G.S. (1988). Measurement of non-uniform residual stresses using the hole-drilling method. *J Eng Mater Technol*, **110: 4**, Part I: 338–343, Part II: 344–349.
9. Aoh, J., Wei, C. (2002). On the Improvement of Calibration Coefficients for Hole-Drilling Integral Method: Part I, Analysis of Calibration Coefficients Obtained by a 3-D FEM Model. *J. Eng. Mater. Technol*, **124: 2**, 250.
10. Aoh, J., Wei, C. (2003). On the Improvement of Calibration Coefficients for Hole-Drilling Integral Method: Part II, Experimental Validation of Calibration Coefficients. *J. Eng. Mater. Technol*, **125: 2**, 107-115.
11. Nicoletto, G. (1991). Moiré interferometry determination of residual stresses in the presence of gradients. *Exp Mech*, **31: 3**, 252–256.
12. Wu, Z., Lu, J., Han, B. (1998). Study of residual stress distribution by a combined method of moiré interferometry and incremental hole drilling. *J Appl Mech*, **65: 4**: Part I: 837–843, Part II: 844–850.
13. Steinzig, M., Ponslet, E. (2003). Residual stress measurement using the hole drilling method and laser speckle interferometry: Part I. *Exp Tech*, **27: 3**, 43–46.
14. Díaz, F.V., Kaufmann, G.H., Möller, O. (2001). Residual stress determination using blind-hole drilling and digital speckle pattern interferometry with automated data processing. *Exp Mech*, **41: 4**,319–323.
15. Nelson, D.V., Makino, A., Schmidt, T. (2006). Residual stress determination using hole drilling and 3D image correlation. *Exp Mech*, **46: 1**, 31–38.
16. Liu, X., Rapik Saat, M., Barkan, C. P. L. (2012). Analysis of causes of major train derailment and their effect on accident rates. *Transportation Research Record: Journal of the Transportation research board*, 2289.
17. Kerr, A. (1978). Analysis of thermal track buckling in the lateral plane. *Acta Mechanica*, **30**, 17–50.
18. Kirsch, E. G. (1898). Die Theorie der Elastizität und die Bedürfnisse der Festigkeitslehre. *Zeitschrift des Vereines deutscher Ingenieure*, **42**, 797–807.
19. Fischer, F.D., Schleinzer, G. (2002). Residual stress formation and distortion of rail steel. *Handbook of residual stress and deformation of steel*, ASM International.